

LARNet: Lie Algebra Residual Network for Profile Face Recognition

Xiaolong Yang¹

Abstract

Due to large variations between profile and frontal faces, profile-based face recognition remains as a tremendous challenge in many practical vision scenarios. Traditional techniques address this challenge either by synthesizing frontal faces or by pose-invariants learning. In this paper, we propose a novel method with Lie algebra theory to explore how face rotation in the 3D space affects the deep feature generation process of convolutional neural networks (CNNs). We prove that face rotation in the image space is equivalent to an additive residual component in the feature space of CNNs, which is determined solely by the rotation. Based on this theoretical finding, we further design a Lie algebraic residual network (LARNet) for tackling profile-based face recognition. Our LARNet consists of a residual subnet for decoding rotation information from input face images, and a gating subnet to learn rotation magnitude for controlling the number of residual components contributing to the feature learning process. Comprehensive experimental evaluations on frontal-profile face datasets and general face recognition datasets demonstrate that our method consistently outperforms the state-of-the-arts.

1. Introduction

The emergence of recent deep learning models and various datasets greatly advanced the frontier of face recognition (Liu et al., 2017; Wang et al., 2018; Deng et al., 2019). Although many deep models are strong and robust to face verification conducted in unconstrained environments, profile face or large pose face recognition still suffers from poor performance (Cao et al., 2018a). It has been evidenced that confronting face recognition in the wild remains to be a significant challenge, because of its data-driven nature (Huang et al., 2016). First of all, since the generalization ability of the deep model is usually proportional to the size of the training data, given an uneven and insufficient distribution of frontal and profile face, the features tend to focus on the frontal one, and the learning results are only biased incomplete statistics. In order to tackle this dilemma, some works

have reconstructed suitable datasets (Masi et al., 2016b) or taken a set of images as input (Xie & Zisserman, 2018) to reduce the need for profile data, but the lack of deep mining limits their performance. Furthermore, there exists other works devoted to combining more dimensions of data information, including multi-task learning (AbdAlmageed et al., 2016; Masi et al., 2016a; Yin & Liu, 2017) or template adaptation (Hassner et al., 2016; Crosswhite et al., 2018). Those strategies tend to increase computational cost and cannot give intuitive and convincing explanations. Some approaches use profile face to synthesize frontal face so that they may avoid large pose variant (Tran et al., 2017; Yin et al., 2017; Zhou et al., 2020). Although frontal face synthesis have assurance of view consistency, such methods would suffer from artifacts caused by occlusions and non-rigid expressions.

We observe that the key to face recognition is to explore the relationship between frontal and profile face. We know that the frontal-profile pair is generated by head rotation, hence we hypothesize that their corresponding deep features may also have this rotation relationship. An existing representative work, called Deep Residual Equivalent Mapping (DREAM) (Cao et al., 2018a) has discussed the gap of those features of frontal-profile pair, but it just uses the learning model to forcibly approximate the difference. More general speaking, it is similar to generative adversarial network (GAN), and makes the target sample (frontal face feature) and the generated sample (profile face feature) as close as possible through encoding and decoding. Without more in-depth understanding and analysis of the relationship, performances are limited by feature representation and need further improvement.

Considering that the rotation matrix is closed under multiplication but not closed under addition, all parts involving numerical calculations cannot introduce rotation and this is a fatal problem for CNNs, which often use gradient descent or perform iterative updates while addition appears everywhere. Benefiting from the classic pose estimation work (Tuzel & abd Peter Meer, 2008) in the *simultaneous localization and mapping* (SLAM), we develop a novel tool Lie group and Lie algebra theory to achieve the rotation in CNN.

The proposed *Lie Algebra Residual Network* (LARNet) is

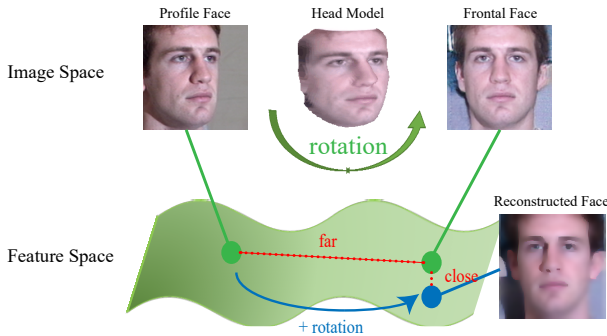


Figure 1. The 'frontalization' or 'rotation' in feature space. Naturally in the real world, the frontal-profile pair is generated by head rotation. We prove that the face rotation in image space is equivalent to an additive residual component in deep feature space. To show the equivalence, we reconstruct the image corresponding to the modified feature (blue dot) and provide the visual result of the frontal face.

conceptually related to the face frontalization or rotation-and-render in that our approach also performs *frontalization* or *rotation* but in the feature space, as shown in Fig.1. We prove that there is a rotation-based relationship between the features of the frontal-profile pair using Lie algebra, and design a corresponding residual transformation function, to realize the mapping between the features of frontal face and profile face. To our best knowledge, this is the first attempt to explore and explain the physical relationship between the features of the frontal face and the profile face theoretically. Meanwhile, we conduct comparative experiments with more than 30 solutions on various evaluation criteria and metrics, while our method outperforms representative state-of-the-art competitors. In summary, our contributions are threefold:

1. We theoretically prove that the features of frontal-profile pair have a physical relationship based on rotation in residual network using Lie Algebra, which is equivalent to an additive residual component in deep feature space of CNNs.
2. We design a novel gating subnet based on the proof, which dose not need to modify the original basic network structure or auxiliary of a large number of modules but brings significant performance improvement.
3. LARNet enhances the model's ability of feature representation and feature classification, and has better performance on various datasets and evaluation criteria, including frontal-profile face verification-identification task and general face recognition task.

2. Related Work

We briefly discuss the most related work of profile face recognition and large pose face recognition.

Insufficient dataset. Masi *et al.* (2016b) propose a more accessible means of increasing training data sizes for face recognition systems: Domain specific data augmentation, and focus on important facial appearance variation. Multi-column Network (Xie & Zisserman, 2018) and Neural Aggregation Network (NAN) (Yang *et al.*, 2017) try to use more information, such as a set of images or videos as input, to tackle the potential shortcomings of a single image. These methods have made some progress, but still far from enough. They tend to falsely match profile faces of different identities and miss frontal and profile faces of the same identity.

Pose variation. Many existing methods have conducted in-depth research on large pose. Template-adaptation-based works (Hassner *et al.*, 2016; Crosswhite *et al.*, 2018) mainly focus on transfer learning by constructed classifier and synthesizer, and pool based on image quality and head pose. As opposed to those techniques which expect a template model to learn pose invariance, pose aware deep learning methods (AbdAlmageed *et al.*, 2016; Masi *et al.*, 2016a) use multiple pose-specific models and rendered face images, which reduce the sensitivity to pose variations. More works favor using more labels instead of pose itself. Multi-task learning (MTL) is widely used, which consists of pose, illumination, and expression (PIE) estimations. Yin *et al.* (2017) propose a pose-directed multi-task CNN and unite the balance of different tasks. DebFace (Zhou *et al.*, 2020) (de-biasing adversarial network) additionally takes gender, age and race into consideration, and minimizes the correlation among feature factors so as to abate the bias influence from other factors. Although these methods are effective, they will increase the computational cost due to the use of multiple models and tasks, and the accuracy of the results cannot meet higher requirements.

Frontalization. Since the profile and large pose bring more challenges, some methods directly use the existing dataset to synthesize the frontal face to perform face recognition. Due to the widespread use of GAN, FF-GAN (Yin & Liu, 2017) and DR-GAN (Tran *et al.*, 2017) surpass the performance of many competitors, with disentangled encoder-decoder structure for learning a generative and discriminative representation. With the rapid progress of 3D face reconstruction technology, the projecting rendering of the frontal face after reconstruction has also risen. Rotate-and-Render (Zhou *et al.*, 2020) is a representative work from single-view images, and can leverage the recent advances in 3D face modeling and high-resolution GAN to constitute building blocks, since the 3D rotation-and-render of faces can be applied to arbitrary angles without losing details. Note that the reconstruction and synthesis only serve for better visualization performance, but they still remain relatively poor feature representation when fully validated through examining performance on face recognition task.

Feature. Some works consider the features rather than the image itself. Shi *et al.* (2019) propose *Probabilistic Face Embeddings* (PFEs), which represent each face image as a Gaussian distribution in the latent space. Feature Transfer Learning (Yin *et al.*, 2019) encourages the under-represented distribution to be closer to the regular distribution. Both of these two try their best to make the sample distribution tend to a Gaussian prior. Although they are aware of paying attention to the feature, specific datasets or face recognition in the real world cannot guarantee that samples should be Gaussian distribution, thus they are lack of intuition and persuasiveness accepted by users. It is worth mentioning another representative work, DREAM (Cao *et al.*, 2018a), which uses the residual network to directly modify the feature of the profile face to the frontal one and looks similar to our work. However, DREAM only considers the gap between the frontal and profile faces, and directly bridges them through a mapping from deep learning. Thus its error will be composed of the feature representation ability and the approximation of the mapping, which is more complex than problem itself. Due to the lack of an in-depth analysis of potential physical relationship between the frontal and profile faces, it can neither achieve accurate feature representation of different pose variants, nor reasonably explain that the learned residual block can be adapt to different identities. Hence, their results reach a bottleneck of feature-representation-based works.

3. Methodology

In this section, we assume that the front face and profile face have a corresponding rotation relationship in the original 3D space. For ease of understanding, only the rotation with the orthogonal transformation relationship is discussed here. The derivation of the more complex Euclidean transformation relationship, including translation and zooming, is referred to the supplementary material.

3.1. Problem Formulation

Our goal is to find a transformation between the features of the input profile face image and expected frontal face image, to realize the *frontalization* in deep feature space and to achieve a robust feature representation to pose variant, as shown in Fig.1.

We denote $\mathcal{F}(\cdot)$ as a feature extraction function in CNNs, and for an image \mathbf{x} , vector $\mathcal{F}(x) \in \mathbb{R}^d$, and d is the dimension of layers considered. We hope to prove that there exists a mapping $\mathcal{R}_{map}(\cdot) : \mathbb{R}^d \rightarrow \mathbb{R}^d$ that it can realize feature representation of the geometric rotation \mathbf{R} of the image \mathbf{x} in the deep feature space:

$$\mathcal{F}(\mathbf{R} \cdot \mathbf{x}) = \mathcal{R}_{map}(\mathcal{F}(\mathbf{x})) \quad (1)$$

Based on our rotation hypothesis, for the frontal face image

\mathbf{x}_f and profile face image \mathbf{x}_p , the homography transformation matrix of two images degenerates into a rotation matrix: $\mathbf{x}_f = \mathbf{R} \cdot \mathbf{x}_p$, and we have:

$$\mathcal{F}(\mathbf{x}_f) = \mathcal{F}(\mathbf{R} \cdot \mathbf{x}_p) = \mathcal{R}_{map}(\mathcal{F}(\mathbf{x}_p)) \quad (2)$$

Furthermore, we use the Lie group theory (Rossmann, 2002) and prove that the mapping can be decomposed into an additive residual component, which is only determined by the rotation:

$$\mathcal{F}(\mathbf{x}_f) = \mathcal{F}(\mathbf{x}_p) + \omega(\mathbf{R}) \cdot \mathbf{C}_{res}(\mathbf{R}, \mathbf{x}_p) \quad (3)$$

Thus we only need a residual subnet \mathbf{C}_{res} for decoding pose variant information from the input face image, and a gating subnet ω to learn rotation magnitude for controlling the amount of residual component contributing to the feature learning process. Eq. (3) is the core principle of LARNet we proposed, and the detailed proof and experimental design will be explained in the following.

3.2. Rotation in Networks and Lie Algebra

To find what the \mathcal{R}_{map} exactly is, we have tried to directly explore and analyze the role of rotation \mathbf{R} in networks from Eq. (2). From the original paper of ResNet (He *et al.*, 2016), it proposes a novel *shortcut*, which not only retains the depth of the network, but also has the advantages of the shallow network to avoid the degradation problem. The learning feature from shallow layer l to deep layer L is as following:

$$\mathbf{x}_L = \mathbf{x}_l + \sum_{i=l}^{L-1} F(\mathbf{x}_i, w_i) \quad (4)$$

$$\begin{aligned} \frac{\partial \text{Loss}}{\partial \mathbf{x}_{l+1}} &= \frac{\partial \text{Loss}}{\partial \mathbf{x}_L} \cdot \frac{\partial \mathbf{x}_L}{\partial \mathbf{x}_l} \\ &= \frac{\partial \text{Loss}}{\partial \mathbf{x}_L} \left(1 + \frac{\partial}{\partial \mathbf{x}_l} \sum_{i=l}^{L-1} F(\mathbf{x}_i, w_i) \right) \end{aligned} \quad (5)$$

where \mathbf{x}_l and \mathbf{x}_{l+1} are represent the input and output vectors of the l -th residual unit respectively, and $F(\cdot)$ is the residual function with weights w . Because the second item in brackets of eq. (5) will quickly drop to a small amount, we focus on the first principal item.

However, in our problem context, it is challenging that involves 3D geometric changes \mathbf{R} with networks. Without loss of generality, we assume that \mathbf{R} is orthogonal and $\in SO(3)$. $SO(3)$ is not a vector space, which means adding two rotation matrices does not result in a valid rotation matrix and the zero matrix $\mathbf{0} \notin SO(3)$. This is a fatal problem for CNNs, because non-linear optimization requires addition, derivative and norms in vector space to define distance or error. Furthermore, it is not guaranteed that the original

rotation relationship will be preserved at each iteration. So we cannot substitute the rotation relationship $\mathbf{x}_f = \mathbf{R} \cdot \mathbf{x}_p$ into eq. (4) and eq. (5) in every block.

Inspired by pose estimation work (Tuzel & abd Peter Meer, 2008) in SLAM, we use the Lie algebra with its own addition, multiplication and derivative to replace the rotation in networks. First, we establish a correspondence between Lie algebra $\phi \in \mathbb{R}^3$ and the rotation $\mathbf{R} \in \mathbb{R}^{3 \times 3}$ based on exponential mapping: $\mathbf{R} = \exp(\phi^\wedge)$, where $^\wedge$ is skew-symmetric operator. And we can solve the Lie algebra through the trace and eigenvalue of rotation matrix by Rodriguez' rotation formula (Rodriguez, 1840) and Taylor expansion:

$$\begin{aligned} \text{tr}(\mathbf{R}) &= \text{tr}(\cos \theta \mathbf{I} + (1 - \cos \theta)\psi\psi^T + \sin \theta\psi^\wedge) \\ &= 2 \cos \theta + 1 \end{aligned} \quad (6)$$

Here $\phi = \theta\psi$ is in Axis-Angle representation form, with a unit vector $\psi \in \mathbb{R}^3$ as the direction of the rotation axis and θ as the rotation angle according to the right hand rule. Besides, for $\mathbf{R}\psi = \psi$, ψ is the eigenvector of \mathbf{R} with corresponding eigenvalue is $\lambda_{\mathbf{R}} = 1$, and we can solve ϕ .

Next, we give the definitions of Lie algebra addition and multiplication with small increment by Baker-Campbell-Hausdorff (BCH) formula (Wulf, 2002; Brian, 2015) and Friedrichs' theorem (Wilhelm, 1954; Jacobson, 1966) :

$$\begin{aligned} \exp(\Delta\phi^\wedge) \exp(\phi^\wedge) &= \exp\left((\phi + \mathbf{J}_l(\phi)^{-1}\Delta\phi)^\wedge\right) \\ \exp((\phi + \Delta\phi)^\wedge) &= \exp((\mathbf{J}_l\Delta\phi)^\wedge) \exp(\phi^\wedge) \end{aligned} \quad (7)$$

\mathbf{J}_l is referred to as the *left Jacobians* of $SO(3)$. And we use the perturbation scheme on Lie group to define derivative, as follows:

$$\begin{aligned} \frac{\partial(\mathbf{R}\mathbf{p})}{\partial(\Delta\phi)} &= \lim_{\Delta\phi \rightarrow 0} \frac{\exp(\Delta\phi^\wedge) \exp(\phi^\wedge) \mathbf{p} - \exp(\phi^\wedge) \mathbf{p}}{\Delta\phi} \\ &= -(\mathbf{R}\mathbf{p})^\wedge \end{aligned} \quad (8)$$

$\mathbf{p} \in \mathbb{R}^3$ is an arbitrary three-dimensional point. Combining eq. (7) with eq. (8), we have the iterative form which makes sense to nonlinear optimization like general gradient descent algorithm:

$$\mathbf{R}\mathbf{p} = \exp(\Delta\phi^\wedge)\mathbf{R}_{\text{init}}\mathbf{p} \approx \mathbf{R}_{\text{init}}\mathbf{p} - (\mathbf{R}_{\text{init}}\mathbf{p})^\wedge\Delta\phi \quad (9)$$

Our scheme guarantees that it will iterate to convergence, and $\mathbf{R}_{\text{init}} \in SO(3)$ always holds at each iteration.

Back to the original problem, given eq. (7) (8) and (9), we

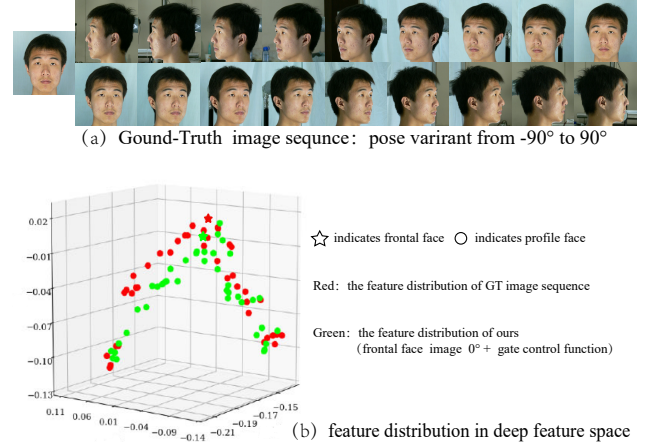


Figure 2. The effect of our gating control function for the same identity. (a) The top is a sequence of images taken in real life, with pose variant form -90° to 90° for the same individual. (b) The bottom is the feature distribution in the deep feature space. The dots represent the profile faces while stars are frontal faces. The red dots are the feature vectors generated by the image sequence, and the green dots are the feature vectors of frontal face image (0°) and yaw angle variant simulated by our gating control function. Their similar distributions can indicate that our gating control function maps the features between the frontal face and the profile face, and improve the feature representation of pose variant.

can rewrite the first principal item of eq. (5) as follows:

$$\begin{aligned} \frac{\partial \text{Loss}}{\partial \mathbf{x}_f} &\approx \lim_{\delta \rightarrow 0} \frac{\text{Loss}}{\exp((\phi + \delta)^\wedge) \cdot \mathbf{x}_p - \exp(\phi^\wedge) \mathbf{x}_p} \\ &= \frac{\partial \text{Loss}}{-(\mathbf{R} \cdot \mathbf{x}_p)^\wedge \cdot \partial \delta} \\ &= \frac{\partial \text{Loss}}{\partial \mathbf{R} \cdot \mathbf{x}_p} \end{aligned} \quad (10)$$

It proves that in the optimizable sense, after adding perturbation \mathbf{R} to \mathbf{x}_p , the result and original input \mathbf{x}_f have the same convergent form at each layer. In fact, since $\mathbf{R} \in SO(3)$, they are asymptotically stable according to Lyapunov's second method (Lyapunov, 1992; Bhatia & Szegö, 2002). With the gradual progress of the ResNet, their feature vectors have the same convergence representations. Furthermore, we decouple the rotation relation from face feature by eq. (6) and eq. (9). So we have:

$$\mathcal{F}(\mathbf{x}_f) \approx \mathcal{F}(\mathbf{x}_p) + \text{Error}_{\mathbf{R}} \cdot \text{Error}_{\text{res}} \quad (11)$$

This is exactly the eq. (3) we mentioned earlier. And we design a gating control function $\omega(\cdot)$ as $\text{Error}_{\mathbf{R}}$ to filter feature flow which related to rotation, and $\text{Error}_{\text{res}}$ is a component obtained through residual network learning and denoted \mathbf{C}_{res} . In our problem context, ω needs to satisfy the following properties:

- $\omega \in [0, 1]$. Intuitively, when the input is frontal face input \mathbf{x}_0 , there is almost no difference in the feature representation

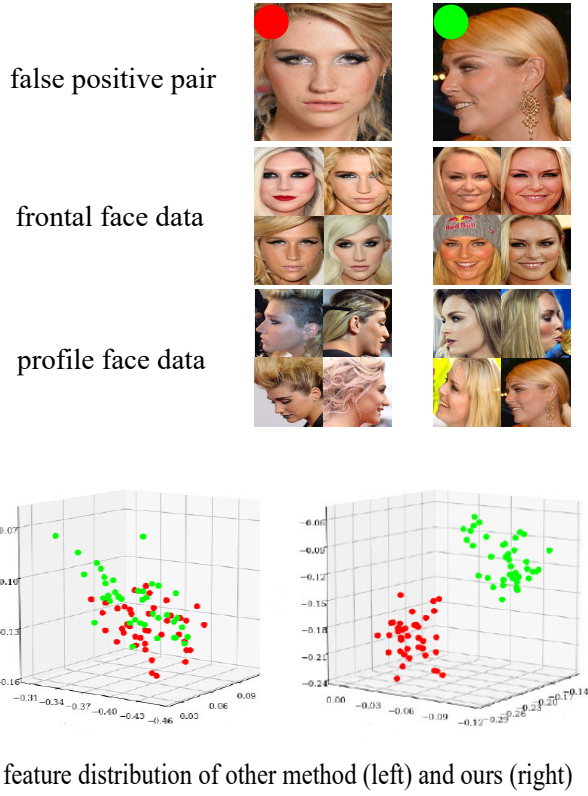


Figure 3. The effect of our gating control function for different identities. This is a challenging false positive example for general face recognition model (Wang et al., 2018). We collect more frontal and profile face data of those two individuals from Celebrities Frontal-Profile dataset (Sengupta et al., 2016), and visualize feature distribution of all the images. It is obvious that our model with gating control function has a better classification and cluster ability.

in the same network, and the C_{res} of the residual learning will bring errors and reduce the classification ability. Therefore, it is hoped that the gating control function is 0 at this time; Ideally, the residual's magnitude is thus the largest at the complete profile pose: $\mathcal{F}(\mathbf{x}_0) - \mathcal{F}(\mathbf{x}_{\pi/2})$, so when the maximum value of the gating control function is 1 :

$$\mathcal{F}(\mathbf{x}_0) = \mathcal{F}(\mathbf{x}_{\pi/2}) + 1 * (\mathcal{F}(\mathbf{x}_0) - \mathcal{F}(\mathbf{x}_{\pi/2})) = \mathcal{F}(\mathbf{x}_0)$$

• ω has symmetric weights. A gating subnet to learn rotation magnitude for controlling the amount of residual component contributing to the feature learning process, and the same deflection angle should have the same influence (for example, yaw angle with turning left or right). We will also use data flipping augmentation to strengthen the symmetry of the model during training.

As a way to demonstrate the effectiveness of our gating control function, Fig. 2 illustrates for the same identity. When inputs are image sequences of the same individual with different yaw angles, ResNet can extract features and display the distribution of those vectors as red dots. Meanwhile, we

use our gating control function with the only frontal face image to simulate pose variant. Our results distribution is marked with green dots. Through the visualization display, it can be clearly seen that our model can accurately simulate the feature vector distribution of different faces varying from yaw angles, which proves that our gating control function improves the feature representation of pose variant.

Fig. 3 also illustrates the effect of our gating control function for different identities. This is a challenging example even for almost blameless face recognition model (Wu et al., 2016). We collect more frontal and profile face data of those two individuals, and visualize feature vectors of all the images corresponding to this sample. It is obvious that our model with gating control function has a better classification and cluster ability.

3.3. Architecture of LARNet

Base Network : Inspired by some network theory researches, such as Saxe et al.’ work (2014), Highway Networks (Srivastava et al., 2015) and Balduzzi et al.’ work (2017), ResNet-50 is the network with the best layers after weighing efficiency and accuracy. Moreover, we find that ResNet-50 is very popular in a large number of existing works, and is very convenient to compare. So we choose ResNet-50 combined margin framework as our baseline, which proposed by ArcFace and loss function is combining all of the margin penalties of SphereFace (Liu et al., 2017), CosFace (Wang et al., 2018) and ArcFace (Deng et al., 2019).

LARNet : The most convenient way of deploying equation (3) is adding the gating control residuals directly to the existing Base Network as a plug-in. Residual learning can be just put before the final fully-connected(FC) layer of the ResNet-50 without changing any learned parameters of the original model. And our residual learning has two fully-connected layers with Parametric Rectified Linear Unit (PReLU) (He et al., 2015) as the activation function. This is trained separately using stochastic gradient descent. As for rotation angle, we take rotation estimation by the state-of-the-art work (Yang et al., 2019; 2020). Taking into account the face alignment before the training, in fact, not all angles have the greatest impact. Hence, in the experiment, we solve equation (6) and use $\sin(\cdot)$ for each component of rotation angle with a $L - \infty$ norm for the constraint parameter, and $\omega = |\sin \theta|$ with $\sin \theta = \|\sin_{pitch}, \sin_{yaw}, \sin_{roll}\|_\infty$.

LARNet+ : Similar to DREAM (Cao et al., 2018a), we also use end-to-end to further improve the performance of our results. Based on LARNet, we make residual learning together with the base network in an end-to-end manner. We train the ResNet and residual learning together and then train the residual learning separately with pose variant frontal-profile face pairs.



Figure 4. Data prepossessing on frontal and profile face. (a) Face flipping: data enhancement for strengthening model’s ability to learn symmetry; (b) Face alignment: reduce the impact caused by translation and rotation in a plane such that the eyes lie along a horizontal line; (c) Face scaling: reduce the impact caused by zooming because focal length is different of every image such that they are approximately identical in size.

4. Experimental Results

In this section, we first list all the datasets used in the experiments and briefly explain their own characteristics (Sec. 4.1). Furthermore, we present two ablation studies on the architecture and gating control function respectively, which explain the contribution of experimental design to recognition performance (Sec. 4.2). We also compare with existing methods and some findings about the profile face representations, conduct detailed experiments on frontal-profile face verification-identification tasks and general face recognition task (Sec.4.3).

4.1. Datasets Exhibition

Training data : We separately employ the two most widely used face datasets as training data in order to conduct fair comparison with other methods, cleaned MS-Celeb-1M database(**MS1MV2**) (Guo et al., 2016) and **CASIA-WebFace** (Yi et al., 2014). MS1MV2 is a clean version of the original MS-Celeb-1M face dataset that has too much mislabeled images, containing 5.8M images of 85,742 celebrities. CASIA-WebFace uses tag-similarity clustering to remove noise of data source, containing 500K images of 100K celebrities from IMDb.

Testing data : We explore many efficient face verification datasets for testing. Celebrities in Frontal-Profile (**CFP**) (Sengupta et al., 2016) is a challenging frontal to profile face verification dataset, containing 500 celebrities, each of which has 10 frontal and 4 profile face images. We extensively test another challenging dataset IARPA Janus Benchmark A (**IJB-A**) (Klare et al., 2015) that covers extreme poses and illuminations, containing 500 identities with 5,712 images and 20,414 frames extracted from videos. Besides focusing on frontal-profile face verification, we also conduct experiments on the general face recognition datasets to verify that our method can reach the state-of-the-art for general face recognition tasks. Including the most widely used **LFW** (Huang et al., 2008) dataset (13,233 face images from 5749 identities) and **YTF** (Wolf et al., 2011) dataset (3,425 videos of 1,595 different people), we also report

Table 1. Ablation study on architecture. Evaluation is conducted on CFP-FP Dataset.

Architectures	Verification(%)
Baseline	92.96
LARNet	98.84
LARNet+	99.21

Table 2. Ablation study on gating control function. Evaluation is conducted on CelebA with metric Equal Error Rate .

Gating Control Function	EER
Identity mapping: $\omega \equiv 1$	15.35
Linear mapping: $\omega = 2\theta/\pi$	9.68
Nolinear mapping: $\omega = \text{sigm}(4\theta/\pi - 1)$	8.45
PReLU	9.72
cReLU with OW	7.92
LARNet: $\omega = \sin \theta $	6.26

the performance of Cross-Pose LFW (**CPLFW**) (Zheng & Deng, 2018), which deliberately searches and selects 3,000 positive face pairs with pose difference to add pose variation to intra-class variance and so the effectiveness of several face verification methods can be fully justified. Furthermore, we also extensively conduct a more in-depth ablation experiment on Large-scale CelebFaces Attributes (**CelebA**) Dataset (Liu et al., 2015b), containing 10,177 celebrities and 202,599 face images, which covers large pose variations.

Data prepossessing is shown in Fig. 4. We use flipping to achieve data enhancement and strengthen our model’s ability to learn symmetry. In addition, face alignment and scaling (224×224) are taken to reduce the impact caused by translation and zooming, when we only consider $SO(3)$ instead of $SE(3)$.

4.2. Ablation Studies

In order to prove that the proposed LARNet does improve the performance of profile face recognition, we implement two ablation experiments: 1. the architectures with the gating control function, 2. the form of the gating control function.

4.2.1. THE ARCHITECTURE OF LARNET.

In this subsection we study the effectiveness of architectures with and without the gating control function as well as an end-to-end optimized manner. From Table. 1, we observe that compared with the strong baseline without gating control function, our LARNet brings a significant advancement 5.88%. And LARNet+ with end-to-end optimized manner also plays a role in further improvement.

Table 3. Quantitative evaluation on IJB-A Dataset. And o.s. denotes optimal setting, while f. is fine tuning/refine. Symbol ‘-’ indicates that the metric is not available for that protocol.

Methods	TAR@FAR=0.01	TAR@FAR=0.001	Rank-1	Rank-5
Wang <i>et al.</i> (2016)	0.729	0.510	0.822	0.931
Pooling Faces (Hassner <i>et al.</i> , 2016)	0.819	0.631	0.846	0.933
Multi Pose-Aware (AbdAlmageed <i>et al.</i> , 2016)	0.787	—	0.846	0.927
DCNN Fusion (f.) (Chen <i>et al.</i> , 2016)	0.838	—	0.903	0.965
PAMs (Masi <i>et al.</i> , 2016a)	0.826	0.652	0.840	0.925
Augmentation+Rendered (Masi <i>et al.</i> , 2016b)	0.886	0.725	0.906	0.962
Multi-task learning (Yin & Liu, 2017)	0.787	—	0.858	0.938
TPE(f.) (Sankaranarayanan <i>et al.</i> , 2017)	0.900	0.813	0.932	—
DR-GAN (Tran <i>et al.</i> , 2017)	0.831	0.699	0.901	0.953
FF-GAN (Yin <i>et al.</i> , 2017)	0.852	0.663	0.902	0.954
NAN (Yang <i>et al.</i> , 2017)	0.921	0.861	0.938	0.960
Multicolumn (Xie & Zisserma, 2018)	0.920	—	—	—
VGGFace2 (Cao <i>et al.</i> , 2018b)	0.904	—	—	—
Template Adaptation(f.) (Crosswhite <i>et al.</i> , 2018)	0.939	—	0.928	—
DREAM (Cao <i>et al.</i> , 2018a)	0.872	0.712	0.915	0.962
DREAM(E2E+retrain,f.) (Cao <i>et al.</i> , 2018a)	0.934	0.836	0.939	0.960
FTL with 60K parameters (o.s.) (Yin <i>et al.</i> , 2019)	0.864	0.744	0.893	0.947
PFEs (Shi & Jain, 2019)	0.944	—	—	—
DebFace (Gong <i>et al.</i> , 2020)	0.902	—	—	—
Rotate-and-Render (Zhou <i>et al.</i> , 2020)	0.920	0.825	—	—
LARNet	0.941	0.842	0.936	0.968
LARNet+	0.951	0.874	0.949	0.971

4.2.2. THE GATING CONTROL FUNCTION.

And we further analyze that what kind of gating control function has a greater contribution to the performance. For facilitating fair comparison, the training settings are CASIA-WebFace dataset and ResNet-50, and evaluation is conducted on CeleA with metric Equal Error Rate (EER). In Table. 2, identity mapping means $\omega \equiv 1$, which represents some GAN-based works, ignoring the internal connection of the frontal-profile face, and only relying on the generator and the discriminator to produce results. Linear mapping: $\omega = 2\theta/\pi$ is a natural attempt and meets the design constraints. Besides, in essence, our gating control function also acts as a filtering activation function, and we compare with two widely used activation function PReLU (He *et al.*, 2015) and cReLU with OW (Balduzzi *et al.*, 2017). Nolinear mapping: $\omega = \text{sigm}(4\theta/\pi - 1)$ is reported by DREAM(Cao *et al.*, 2018a). And our method $\omega = |\sin \theta|$ still achieves the best result: EER 6.26. This observation ascertains our design of exerting a higher degree of correction to a profile face, and has a better understanding of the effectiveness of our LARNet on profile face recognition.

4.3. Quantitative Evaluation Results

We compare our method with more than 30 excellent work with different loss functions from 2016 to 2020, which covers template based, GAN, residual learning, three-

dimensional reconstruction and other method systems, aiming at various tasks such as face search, face recognition, face verification, large pose recognition, etc. All numerical datas are the best results obtained from original quotation, cross-reference, and experimental reproduction.

4.3.1. IJBA DATASET: VERIFICATION AND IDENTIFICATION TASKS WITH STATE OF THE ART.

In this experiment, we evaluate our method on challenging benchmark IJBA that covers full pose variation and complies with the original standard protocol. The evaluation metrics are popular True Acceptance Rate (TAR) at False Acceptance Rate (FAR) of 0.01 and 0.001 on the verification task, and Rank-1/Rank-5 recognition accuracy on the identification task. The training settings are MS1MV2 dataset and ResNet-50.

In Table. 3, we compare with various the state-of-the-art techniques. Our LARNet reaches 0.941 (TAR@FAR=0.01), and after refinement with end-to-end retrain, LARNet+ achieves better performance with 0.951. They have surpassed other existing methods by a large margin. These our methods also bring significant improvement on more challenging TAR@FAR=0.001, with 0.842 and 0.874 respectively. Furthermore, as for face identification, LARNet has an advantage in both Rank-1 (0.936) and Rank-5 (0.968), and LARNet+ pushes the result to a higher level: Rank-

Table 4. Quantitative Evaluation on CFP-FP Dataset. And o.s. denotes optimal setting, while f. is fine tuning/refine.

Methods	Verification(%)
SphereFace (o.s.+f.)	94.17
CosFace (o.s.)	94.40
ArcFace (o.s.+f.)	94.04
URFace(all modules, MS1MV2, o.s.)	98.64
Human-level	98.92
LARNet	98.84
LARNet+	99.21

1 (0.949) and Rank-5 (0.971). Our method has achieved advanced performance in both recognition and verification.

4.3.2. CFP-FP DATASET: PROFILE FACE VERIFICATION CHALLENGE

We employ CFP-FP as the frontal profile face verification dataset with the protocol that the whole dataset is divided into 10 folds each containing 350 same and 350 not-same pairs of 50 individuals. From Table 4, we can find that the face verification results of state-of-the-art face recognition models are basically at 94%+. It is worth noting that in 2020, the latest work - universal representation learning face work (URFace) (Shi et al., 2020), has reached an astonishing 98.64% under the training of MS1MV2 dataset and the auxiliary learning of a large number of modules, such as variation augmentation, confidence-aware identification loss, and multiple embeddings. However, the result of our LARNet has reached 98.84%, which outperforms almost all competitors. As for further advanced LARNet+, to our best knowledge, the 99.21% performance is the first to surpass the reported human-level performance (98.92%) on this CFP-FP dataset.

4.3.3. LFW, YTF AND CPLFW DATASETS: GENERAL FACE RECOGNITION.

To get a better understanding of our LARNet’s superiority, we conduct a more in-depth comparison on general face recognition. LFW and YTF datasets are the most widely used benchmark for unconstrained face verification on images and videos. In this paper, we follow the unrestricted with labelled outside data protocol to report the performance. CPLFW emphasizes pose difference to further enlarge intra-class variance. The training settings are CASIA-WebFace dataset and ResNet-50, while results of some different experimental settings (marked with ‘*’) are also reported.

From Table 5, we found that because the LFW dataset is too small, almost all methods can achieve 99+. Although the meaning of this is very weak, the result of our method

Table 5. General Face Recognition Datasets. And o.s. denotes optimal setting, while f. is fine tuning/refine. Symbol ‘-’ indicates that the metric is not available for that protocol. For fairness, the training network and dataset: ResNet50 + CASIA-WebFace. Symbol ‘*’ indicates other training setting.

Methods	LFW	YTF	CPLFW
HUMAN-Individual	97.27	-	81.21
HUMAN-Fusion	99.85	-	85.24
DeepID (Sun et al., 2014)	99.47	93.20	-
Deep Face (Taigman et al., 2014)	97.35	91.4	-
VGG Face (Parkhi et al., 2015)	98.95	97.30	90.57
FaceNet (Schroff et al., 2015)	99.63	95.10	-
Baidu (Liu et al., 2015a)	99.13	-	-
Center Loss (Wen et al., 2016)	99.28	94.9	85.48
Range Loss (Zhang et al., 2017)	99.52	93.70	-
Marginal Loss (Deng et al., 2017)	99.48	95.98	-
SphereFace(o.s.) (Liu et al., 2017)	99.42	95.0	81.4
SphereFace+(o.s.)	99.47	-	90.30
CosFace(o.s.) (Wang et al., 2018)	99.51	96.1	-
CosFace*(MS1MV2,R64, o.s.)	99.73	97.6	-
Arcface(o.s.) (Deng et al., 2019)	99.53	-	92.08
ArcFace*(MS1MV2,R100,f.)	99.83	98.02	95.45
Ours: LARNet	99.36	96.55	95.51
Ours: LARNet+	99.71	97.63	96.23

99.71 is also at the forefront, only inferior to human-level 99.85 and Arcface 99.83, whose training data is MS1MV2 in ResNet-100 with fine tuning. For the video sampled dataset YTF, our LARNet and LARNet+ results are still superior compared with the existing excellent face recognition work. As for the more challenging CPLFW with large pose, which has more realistic consideration on pose intra-class variation, our method has demonstrated our strengths with better results 95.51 and 96.23 respectively.

5. Conclusion

We have proposed a Lie Algebra Residual Network (LARNet) to improve profile face recognition. First, we present a novel method with Lie algebra theory to explore how face rotation in 3D space affects deep feature generation process, and prove that the face rotation in image space is equivalent to an additive residual component in deep feature space, which is only determined by the rotation. Furthermore, we design a gating control function derived using the Lie algebra, which learns rotation magnitude and controls the amount of residual component in feature learning process. And we provide the results of ablation studies to verify the effectiveness of our theory. Compared with various state-of-the-art techniques on extensive datasets, experiments demonstrate the superior performance of our approach on frontal-profile face verification, face identification and general face recognition.

References

AbdAlmageed, W., Wu, Y., Rawls, S., Harel, S., Hassner, T., Masi, I., Choi, J., Lekust, J., Kim, J., Natarajan, P., Nevatia, R., and Medioni, G. Face recognition using deep multi-pose representations. In *IEEE Winter Conference on Applications of Computer Vision (WACV)*, pp. 1–9, 2016.

Balduzzi, D., Frean, M., Leary, L., Lewis, J., Ma, K. W.-D., and McWilliams, B. The shattered gradients problem: If resnets are the answer, then what is the question? In *The International Conference on Machine Learning (ICML)*, 2017.

Bhatia, N. P. and Szegö, G. P. *Stability theory of dynamical systems*. Springer Science & Business Media, 2002.

Brian, H. *Lie groups, Lie algebras, and representations: an elementary introduction*. Springer, 2015.

Cao, K., Rong, Y., Li, C., Tang, X., and Loy, C. C. Pose-robust face recognition via deep residual equivariant mapping. In *IEEE Conference on Computer Vision and Pattern Recognition (CVPR)*, pp. 5187–5196, 2018a.

Cao, Q., Shen, L., Xie, W., Parkhi, O. M., and Zisserman, A. Vggface2: A dataset for recognising faces across pose and age. In *IEEE International Conference on Automatic Face & Gesture Recognition (FG)*, pp. 67–74, 2018b.

Chen, J.-C., Patel, V. M., and Chellappa, R. Unconstrained face verification using deep cnn features. In *IEEE Winter Conference on Applications of Computer Vision (WACV)*, 2016.

Crosswhite, N., Byrne, J., Stauffer, C., Parkhi, O., Cao, Q., and Zisserman, A. Template adaptation for face verification and identification. *Image and Vision Computing*, 79: 35–48, 2018.

Deng, J., Zhou, Y., and Zafeiriou, S. Marginal loss for deep face recognition. In *IEEE Conference on Computer Vision and Pattern Recognition (CVPR) Workshops*, pp. 60–68, 2017.

Deng, J., Guo, J., Xue, N., and Zafeiriou, S. Arcface: Additive angular margin loss for deep face recognition. In *IEEE Conference on Computer Vision and Pattern Recognition (CVPR)*, pp. 4690–4699, 2019.

Gong, S., Liu, X., and Jain, A. K. Jointly de-biasing face recognition and demographic attribute estimation. In *European Conference on Computer Vision (ECCV)*, pp. 330–347, 2020.

Guo, Y., Zhang, L., Hu, Y., He, X., and Gao, J. Ms-celeb-1m: A dataset and benchmark for large-scale face recognition. In *European Conference on Computer Vision (ECCV)*, pp. 87–102, 2016.

Hassner, T., Masi, I., Kim, J., Choi, J., Harel, S., Natarajan, P., and Medioni, G. Pooling faces: Template based face recognition with pooled face images. In *IEEE Conference on Computer Vision and Pattern Recognition (CVPR) Workshops*, pp. 59–67, 2016.

He, K., Zhang, X., Ren, S., and Sun, J. Delving deep into rectifiers: Surpassing human-level performance on imagenet classification. In *IEEE International Conference on Computer Vision (ICCV)*, pp. 1026–1034, 2015.

He, K., Zhang, X., Ren, S., and Sun, J. Deep residual learning for image recognition. In *IEEE Conference on Computer Vision and Pattern Recognition (CVPR)*, pp. 770–778, 2016.

Huang, C., Li, Y., Loy, C. C., and Tang, X. Learning deep representation for imbalanced classification. In *IEEE Conference on Computer Vision and Pattern Recognition (CVPR)*, pp. 5375–5384, 2016.

Huang, G. B., Mattar, M., Berg, T., and Learned-Miller, E. Labeled faces in the wild: A database for studying face recognition in unconstrained environments. In *Workshop on faces in Real-Life Images: detection, alignment, and recognition*, 2008.

Jacobson, N. *Lie Algebras*. John Wiley & Sons, 1966.

Klare, B. F., Klein, B., Taborsky, E., Blanton, A., Cheney, J., Allen, K., Grother, P., Mah, A., and Jain, A. K. Pushing the frontiers of unconstrained face detection and recognition: Iarpa janus benchmark a. In *IEEE Conference on Computer Vision and Pattern Recognition (CVPR)*, pp. 1931–1939, 2015.

Liu, J., Deng, Y., Bai, T., Wei, Z., and Huang, C. Targeting ultimate accuracy: Face recognition via deep embedding. In *arXiv preprint:1506.07310*, 2015a.

Liu, W., Wen, Y., Yu, Z., Li, M., Raj, B., and Song, L. Sphereface: Deep hypersphere embedding for face recognition. In *IEEE Conference on Computer Vision and Pattern Recognition (CVPR)*, pp. 212–220, 2017.

Liu, Z., Luo, P., Wang, X., and Tang, X. Deep learning face attributes in the wild. In *IEEE International Conference on Computer Vision (ICCV)*, pp. 3730–3738, 2015b.

Lyapunov, A. M. The general problem of the stability of motion. *International Journal of Control*, 55(3):531–534, 1992.

Masi, I., Rawls, S., Medioni, G., and Natarajan, P. Pose-aware face recognition in the wild. In *IEEE Conference on Computer Vision and Pattern Recognition (CVPR)*, pp. 4838–4846, 2016a.

Masi, I., Tran, A. T., Hassner, T., Leksut, J. T., and Medioni, G. Do we really need to collect millions of faces for effective face recognition? In *European Conference on Computer Vision (ECCV)*, pp. 579–596, 2016b.

Parkhi, O. M., Vedaldi, A., and Zisserman, A. Deep face recognition. In *British Machine Vision Association*, pp. 1–12, 2015.

Rodriguez, O. Des lois geometriques qui regissent les deplacements d'un systeme solide dans l'espace et de la variation des coordonnees provenant de deplacements consideres independamment des causes qui peuvent les produire. *J Mathematiques Pures Appliquees*, 5:380–440, 1840.

Rossmann, W. *Lie Groups: An Introduction Through Linear Groups*. Oxford Press, 2002.

Sankaranarayanan, S., Alavi, A., Castillo, C. D., and Chellappa, R. Triplet probabilistic embedding for face verification and clustering. In *IEEE International Conference on Biometrics theory, Applications and Systems (BTAS)*, 2017.

Saxe, A. M., McClelland, J. L., and Ganguli, S. Exact solutions to the nonlinear dynamics of learning in deep linear neural networks. In *The International Conference on Learning Representations (ICLR)*, 2014.

Schroff, F., Kalenichenko, D., and Philbin, J. Facenet: A unified embedding for face recognition and clustering. In *IEEE Conference on Computer Vision and Pattern Recognition (CVPR)*, pp. 815–823, 2015.

Sengupta, S., Chen, J.-C., Castillo, C., Patel, V. M., Chellappa, R., and Jacobs, D. W. Frontal to profile face verification in the wild. In *IEEE Winter Conference on Applications of Computer Vision (WACV)*, pp. 1–9, 2016.

Shi, Y. and Jain, A. K. Probabilistic face embeddings. In *IEEE International Conference on Computer Vision (ICCV)*, pp. 6902–6911, 2019.

Shi, Y., Yu, X., Sohn, K., Chandraker, M., and Jain, A. K. Towards universal representation learning for deep face recognition. In *IEEE Conference on Computer Vision and Pattern Recognition (CVPR)*, pp. 6817–6826, 2020.

Srivastava, R. K., Greff, K., and Schmidhuber, J. Highway networks. In *The International Conference on Machine Learning (ICML) Deep Learning workshop*, 2015.

Sun, Y., Chen, Y., Wang, X., and Tang, X. Deep learning face representation by joint identification-verification. In *NeurIPS*, pp. 1988–1996, 2014.

Taigman, Y., Yang, M., Ranzato, M., and Wolf, L. Deepface: Closing the gap to human-level performance in face verification. In *IEEE Conference on Computer Vision and Pattern Recognition (CVPR)*, pp. 1701–1708, 2014.

Tran, L., Yin, X., and Liu, X. Disentangled representation learning gan for pose-invariant face recognition. In *IEEE Conference on Computer Vision and Pattern Recognition (CVPR)*, pp. 1415–1424, 2017.

Tuzel, O. and abd Peter Meer, F. P. Learning on lie groups for invariant detection and tracking. In *IEEE Conference on Computer Vision and Pattern Recognition (CVPR)*, pp. 1–8, 2008.

Wang, D., Charles, O., and Anil, K. J. Face search at scale. *IEEE Transactions on Pattern Analysis and Machine Intelligence (T-PAMI)*, 39(6):1122–1136, 2016.

Wang, H., Wang, Y., Zhou, Z., Ji, X., Gong, D., Zhou, J., Li, Z., and Liu, W. Cosface: Large margin cosine loss for deep face recognition. In *IEEE Conference on Computer Vision and Pattern Recognition (CVPR)*, pp. 5265–5274, 2018.

Wen, Y., Zhang, K., Li, Z., and Qiao, Y. A discriminative feature learning approach for deep face recognition. In *European Conference on Computer Vision (ECCV)*, pp. 499–515, 2016.

Wilhelm, M. On the exponential solution of differential equations for a linear operator. *Communications on Pure and Applied Mathematics*, 7(4):649–673, 1954.

Wolf, L., Hassner, T., and Maoz, I. Face recognition in unconstrained videos with matched background similarity. In *IEEE Conference on Computer Vision and Pattern Recognition (CVPR)*, pp. 529–534, 2011.

Wu, Y., Li, J., Kong, Y., and Fu, Y. Deep convolutional neural network with independent softmax for large scale face recognition. In *Proceedings of the 24th ACM international conference on Multimedia*, pp. 1063–1067, 2016.

Wulf, R. *Lie Groups – An Introduction Through Linear Groups*. Oxford Graduate Texts in Mathematics, Oxford Science Publications, 2002.

Xie, W. and Zisserma, A. Multicolumn networks for face recognition. In *arXiv preprint:1807.09192*, 2018.

Yang, J., Ren, P., Zhang, D., Chen, D., Wen, F., Li, H., and Hua, G. Neural aggregation network for video face recognition. In *IEEE Conference on Computer Vision and Pattern Recognition (CVPR)*, pp. 4362–4371, 2017.

Yang, T.-Y., Chen, Y.-T., Lin, Y.-Y., and Chuang, Y.-Y. Fsa-net: Learning fine-grained structure aggregation for head pose estimation from a single image. In *IEEE Conference on Computer Vision and Pattern Recognition (CVPR)*, pp. 1087–1096, 2019.

Yang, X., Jia, X., Yuan, M., and Yan, D.-M. Real-time facial pose estimation and tracking by coarse-to-fine iterative optimization. *Tsinghua Science and Technology*, 25(5): 690–700, 2020.

Yi, D., Lei, Z., Liao, S., and Li, S. Z. Learning face representation from scratch. In *arXiv preprint:1411.7923*, 2014.

Yin, X. and Liu, X. Multi-task convolutional neural network for pose-invariant face recognition. *IEEE Transactions on Image Processing*, 27(2):964–975, 2017.

Yin, X., Yu, X., Sohn, K., Liu, X., and Chandraker, M. Towards large-pose face frontalization in the wild. In *IEEE International Conference on Computer Vision (ICCV)*, pp. 3990–3999, 2017.

Yin, X., Yu, X., Sohn, K., Liu, X., and Chandraker, M. Feature transfer learning for face recognition with under-represented data. In *IEEE Conference on Computer Vision and Pattern Recognition (CVPR)*, pp. 5704–5713, 2019.

Zhang, X., Fang, Z., Wen, Y., Li, Z., and Qiao, Y. Range loss for deep face recognition with long-tailed training data. In *IEEE International Conference on Computer Vision (ICCV)*, pp. 5409–5418, 2017.

Zheng, T. and Deng, W. Cross-pose lfw: A database for studying cross-pose face recognition in unconstrained environments. In *Technical Report of Beijing University of Posts and Telecommunications*, 2018.

Zhou, H., Liu, J., Liu, Z., Liu, Y., and Wang, X. Rotate-and-render: Unsupervised photorealistic face rotation from single-view images. In *IEEE Conference on Computer Vision and Pattern Recognition (CVPR)*, pp. 5911–5920, 2020.